Review of Combustion Indexes Remote Sensing Applied to Different Combustion Types

Author, co-author (Do NOT enter this information. It will be pulled from participant tab in MyTechZone)

Affiliation (Do NOT enter this information. It will be pulled from participant tab in MyTechZone)

Abstract

This paper summarizes the main studies carried out by the authors for the development of indexes for remote combustion sensing applicable to different combustion types, i.e. conventional gasoline and diesel combustions, diesel PCCI and dual fuel gasoline-diesel RCCI.

It is well-known that the continuous development of modern Internal Combustion Engine (ICE) management systems is mainly aimed at complying with upcoming increasingly stringent regulations throughout the world, both for pollutants and CO2 emissions.

Performing an efficient combustion control is crucial for efficiency increase and pollutant emissions reduction. Over the past years, the authors of this paper have developed several techniques to estimate the most important combustion indexes for combustion control, without using additional cylinder pressure sensors but only using the engine speed sensor (always available on board) and accelerometers (usually available on-board for gasoline engines). In addition, a low-cost sensor based on acoustic sensing can be integrated to support combustion indexes evaluation and other engine relevant information.

The real-time calculation of combustion indexes is even more crucial for innovative Low Temperature Combustions (such as diesel PCCI or dual fuel gasoline-diesel RCCI), mainly due to the high instability and the high sensitivity to slight variations of the injection parameters that characterize this kind of combustions. Therefore, the authors of this paper have applied the developed techniques not only to conventional engines (gasoline and diesel combustion), but also to engines modified for Low Temperature Combustions, with promising results in terms of validation and applicability for real-time combustion control.

The developed methodologies have been tested and validated through a large amount of experimental tests. To run the estimation algorithms in real-time, they have been all implemented in a specifically designed rapid control prototyping system, the goal being to quantify the accuracy of the estimations and optimize the strategy implementations for the extensive use (in the near future) in modern Engine Control Modules (ECM).

Introduction

Due to the increasing request for pollutant emissions reduction in internal combustion engines, a large amount of research has been carried out over the past years to investigate advanced combustion methodologies. In particular, a significant reduction in both NOx and particulate matter, together with efficiency improvement, can be achieved through the use of high EGR rates and innovative Low Temperature Combustion (LTC) strategies, usually characterized by a highly premixed combustion portion.

Even though high EGR rates and LTC strategies proved to be effective to reduce engine-out emissions, the on-board application is limited by their sensitivity to in-cylinder thermal conditions, such as slight variations in the temperature of fresh air charge, cylinder walls and residual gases. Consequently, non-optimal combustion control (based on static maps of the injection parameters) can lead to combustion instability and cylinder-by-cylinder imbalance. To avoid such problems, closed-loop combustion control is necessary [1-3].

Previous works demonstrate that pollutant emissions reduction can be achieved through closed-loop combustion control based on the real-time processing of in-cylinder pressure trace [4-8]. As a matter of fact, a proper processing of this signal provides crucial information about the way combustion takes place in the combustion chamber, such as torque delivered by the engine, pressure peak location, start of combustion (SOC) and crank angle of 50% fuel mass burned (CA50). However, pressure sensors on-board installation is still uncommon, mainly due to problems related to reliability and cost. To overcome such limitations, several remote combustion sensing methodologies have been developed over the past years, the goal being to extract information about combustion through the real-time processing of signals coming from low-cost sensors (both standard and additional) mounted on the engine.

This paper presents the review of several combustion sensing algorithms, developed by the authors over the past years, that can be combined in an overall remote combustion sensing methodology that allows estimating many indicated quantities suitable to feedback closed-loop control strategies, such as:

- Indicated torque delivered by the engine;

- Center of combustion (CA50);

- Start of combustion (SOC);

- Pressure Peak location within the cycle;

- Combustion Noise.

The presented virtual sensing approach is based on the analysis of engine vibration, engine speed fluctuation and engine acoustic emission, therefore the installation of cylinder pressure sensors is not required. Engine speed fluctuations can be derived from the same phonic wheel already mounted on-board for other control purposes (no extra hardware cost), while engine block acceleration and acoustic emission can be measured using an accelerometer mounted on the engine block and a proper microphone (compared to the installation of pressure sensors, the additional hardware cost is much lower).

Previous works [9-11] demonstrate that CA50 (average value over one cycle) and indicated torque delivered by each cylinder can be determined through a proper processing of crankshaft speed fluctuations while the signal coming from the accelerometer mounted on the engine block can be used to determine start of combustion and pressure peak location within the engine cycle (one per cylinder) [11]. In addition, a proper processing of the acoustic emission captured by a microphone-based device can be used to real-time control combustion noise.

This paper proposes novel applications of all the developed approaches to modern engine architectures and innovative combustion techniques, the goal being to provide information about the potential related to the use of remote combustion sensing techniques for the control of internal combustion engines.

The virtual sensors developed and presented in this work are general, therefore can be applied to engines with different architectures and combustions. The estimation algorithms have been implemented in a programmable Rapid Control Prototyping (RCP) system, used to real-time estimate the indicated quantities of interest during the operation of diesel and gasoline engines with different layouts (in terms of combustion order and angular spacing between combustions). In addition, to validate the algorithms for LTC strategies, one Compression Ignited (CI) diesel engine has been also operated in PCCI (diesel) and RCCI (dual fuel with diesel and gasoline) mode.

Experimental Setup

A specific Rapid Control Prototyping (RCP) system has been developed to test the presented combustion sensing strategies. The RCP, based on a National Instruments cRio 9082, acquires (as inputs) all the available sensors of interest, i.e. the signal coming from the standard VRS speed sensor mounted on-board, engine block acceleration and the voltage signal coming from the microphone. Based on the input signals, the RCP system calculates the estimated indicated quantities of interest (through the virtual sensing algorithms that will be discussed in the following sections) and corrects the standard injection/ignition pattern overwriting the commands of the standard ECU via CAN bus (CAN0). If one of the mentioned signals is not available, the estimation algorithms based on that signal are disabled.

Compared to the standard layout of the investigated engines, the experimental layout set up to calibrate and test the algorithms is characterized by several additional sensors. Each cylinder is equipped with one piezo-electric pressure sensor and cylinder pressure traces are acquired and analyzed using an indicating system that real-time calculates all the indicated quantities of interest, i.e. indicated torque, center of combustion (CA50) and pressure peak location. Engine block acceleration is measured using one additional accelerometer

(PCB Piezotronic 352C33) installed in a position in which the block acceleration due to the combustion process can be perceived with a high signal-to-noise ratio (the chosen position depends on the engine architecture taken into consideration). Finally, engine acoustic emission was measured using a microphone-based sensing device, developed by Magneti Marelli. Engine noise signal was also measured using a PCB Teds 378C01 microphone faced to the engine block and acquired at a sample frequency of 100 kHz, as a reference for the acoustic probe [12].

All the signals coming from standard sensors already present on-board for control purposes are monitored and acquired using INCA software and ETAS hardware. The non-standard sensors installed in the test cell are acquired using the test bench controller (TestIT by Alma Automotive) and stored in the Host PC. The scheme of the experimental layout is summarized in Figure 1.
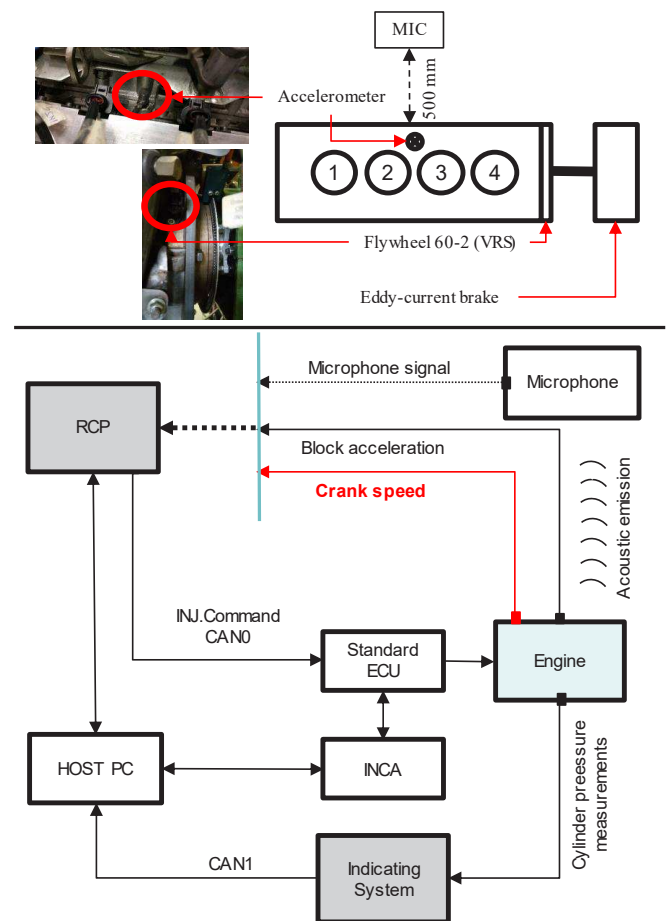

Figure 1. Scheme of the developed experimental setup and sensors installation for the 4-cylinder CI engine.

As already mentioned, all the remote combustion sensing algorithms have been implemented in the RCP system, the goal being to estimate all the main indicated quantities usually calculated from cylinder pressure sensors. The following sections report the results obained analyzing different engine layouts and engine operating modes.

Indicated Torque and CA50 Evaluation via Crankshaft Speed Signal

This section describes the results obtained applying a methodology for CA50 and indicated torque estimation to 2 engines with different engine layouts. The first engine taken into consideration is a 4-cylinder 1.3L compression-ignited (CI) engine that performs four evenly-spaced combustions within the cycle. Then, the same estimation algorithm has been also applied to a 1.0L spark-ignited (SI) gasoline with 4 cylinders in which combustions are not evenly-spaced.

Compression ignited engine with evenly-spaced combustions

The CI engine under study is equipped with a standard diesel Common-Rail injection system, that allows managing up to 8 injections per cycle. The technical characteristics of the standard engine are summarized in Table 1.

Table 1. Engine technical characteristics.

Displaced volume	1248 cc
Maximum Torque	200 Nm @ 1500 rpm
Maximum Power	70 kW @ 3800 rpm
Injection System	Common Rail, Multi-Jet
Bore	69.6 mm
Stroke	82 mm
Compression ratio	16.8:1
Number of Valves	4 per cylinder
Architecture	L4
Firing Order	1-3-4-2

According to previous works [13,14], the correlation existing between the generic k-th frequency components of engine speed and torque applied to the crankshaft can be expressed using a transfer function that only depends on the torsional characteristics of the engine-driveline system. The k-th harmonic component of torque delivered by the engine can be calculated as the difference between the corresponding harmonic components of indicated and reciprocating torque. Indicated torque fluctuation ($T_{ind,k}$) can be directly calculated starting from cylinder pressure measurement, while reciprocating torque fluctuation ($T_{r,k}$) can be calculated as a function of engine speed and reciprocating masses. With regard to the k-th harmonic component of engine speed ($\dot{\theta}_k$), it can be calculated starting from engine speed measurement carried out using the same toothed wheel mounted on-board. Therefore, named $H(j\omega)$ the transfer function, it can be expressed through Eq. (1).

$$H(j\omega) = \frac{T_{ind,k} - T_{r,k}}{\omega \cdot \dot{\theta}_k} \qquad (1)$$

Since the value of the reciprocating masses is not always well known, the consequent errors in the evaluation of the transfer function might be not negligible. This problem has been overcome in previous works by the same authors [10] applying Eq. (1) to a test run in cutoff conditions (no fuel injected) at the same engine speed. The mathematical expression of $H(j\omega)$ can be rearranged as follows:

$$H(j\omega) = \frac{T_{ind,k} - T_{ind\ cutoff,k}}{\omega \cdot (\dot{\theta}_k - \dot{\theta}_{cutoff,k})} \qquad (2)$$

Here, $T_{ind\ cutoff,k}$ and $\dot{\theta}_{cutoff,k}$ represent the k-th harmonics of indicated torque and engine speed measured during an engine cycle run at the same engine speed but in cutoff conditions (no fuel injected). A detailed discussion of the methodology for the identification of the engine-driveline Transfer Function is beyond the scope of this work. However, the complete methodology is widely discussed in literature.

Once Eq. (2) has been determined, the transfer function can be calculated through the analysis of experimental data (torque and speed), but it is necessary to choose the proper k-th harmonic characteristic of the engine. The k-th harmonic of interest is the one at which torque and speed fluctuations show the highest amplitude, i.e. the one corresponding to the order characteristic of the engine. Since the engine used throughout this work performs 4 evenly-spaced combustions per cycle, the harmonic component of interest is k=4. As a matter of fact, if all the cylinders behave the same way, i.e. produce the same torque waveform over crank angle, the only difference between the torque harmonic components will be a phase shift related to the firing order. Therefore, as it can be observed in Figure 2, if the 4 cylinders are perfectly balanced, the torque harmonic components ($T_{ind,k}$) for k=1, 2, 3 will be identically equal to 0.
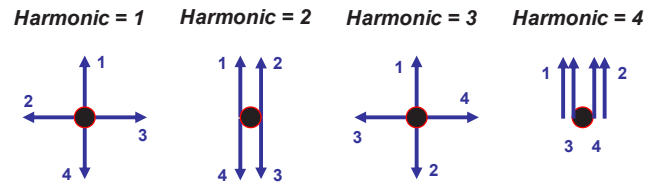

Figure 2. Torque harmonic components up to harmonic 4.

Bearing in mind that only the harmonic component characteristic of the engine needs to be taken into account, the corresponding tranfer function of the engine-brake system has been calculated from transient tests run in CDC mode.
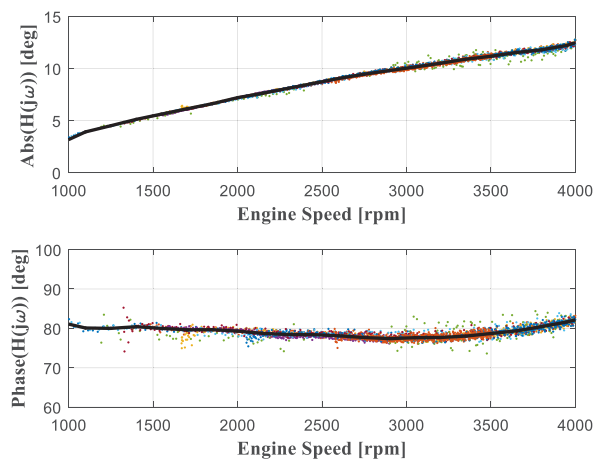

Figure 3. Transfer function characteristic of the CI engine-brake system.

As reported in literature [10], only 3 engine speed ramps run at different load levels (cut-off conditions, medium load and full load) are necessary to calibrate the whole strategy. During the ramp tests, the whole speed range of the engine needs to be explored (from 1000 to approximately 4000 rpm for the 4-cylinder engine under study) to obtain a complete characterization of the transfer function. Amplitude and phase of the obtained transfer function are shown in Figure 3.

Once $H(j\omega)$ has been determined, it can be used for real-time estimation of the indicated torque fluctuation during a generic operating condition simply rearranging Eq. (2) as follows:

$$T_{ind,k} = T_{ind\ cutoff,k} + H(j\omega) \cdot \omega \cdot (\dot{\theta}_k - \dot{\theta}_{cutoff,k}) \qquad (3)$$

With regard to the quantities corresponding to the motored conditions, $\dot{\theta}_{cutoff,k}$ can be measured during a cutoff and stored in a map as a function of engine speed, while $T_{ind\ cutoff,k}$ can be estimated, as a function of manifold pressure and engine speed, through Eq.(4) [10] (both maps have been programmed in the RCP system).

$$abs(T_{ind\ cutoff,k}) = c_0 + k_1 \cdot p_{man} + k_2 \cdot \dot{\theta}_0$$
$$angle(T_{ind\ cutoff,k}) = 90\ [deg] \qquad (4)$$

It is important to highlight that the transfer function (and consequently the estimation of the torque harmonic component) is not affected by the combustion strategy (CDC, PCCI, RCCI, …), since it only depends on the torsional characteristics of the engine-driveline system under investigation [15].

Conventional Diesel Combustion (CDC)

The calculated transfer function demonstrates that the indicated torque component of interest (amplitude and phase) can be estimated starting from the real-time processing of the crankshaft speed signal. Once the indicated torque fluctuation of interest has been determined, it can be used to estimate both indicated torque and center of combustion (CA50). As a matter of fact, previous works by the same authors demonstrate that it is possible to identify a strong correlation between torque fluctuation amplitude and its mean value over the engine cycle (together with the intake manifold pressure p_{man}) as well as between torque fluctuation phase and CA50 (linear correlation) [9]. The analysis of these correlations will not be reported here, but it is fully discussed in literature. The main aspect to be underlined is that both torque delivered by the engine and the center of combustion can be estimated only through the analysis of crankshaft speed fluctuation (carried out using the same phonic wheel already mounted on-board).

The complete methodology for indicated torque and CA50 estimation has been implemented in the RCP and used to real-time estimate these quantities from engine speed measurement. The results obtained during transient tests run in CDC mode are reported in Figure 4.

The estimation methodology proved to be very accurate in CDC mode, therefore the estimated indicated quantities might be used to feedback a closed-loop combustion control strategy.
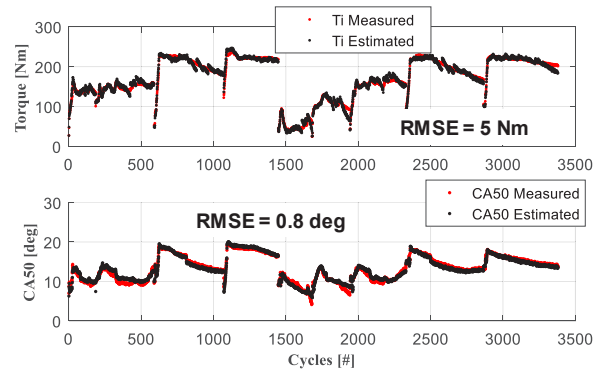

Figure 4: Indicated torque mean value and center of combustion in CDC mode, estimated vs measured.

In this case, a closed-loop combustion control strategy has been also implemented in the RCP. Based on the estimated values of torque and center of combustion, such control strategy dynamically changes the energizing time of the Main injection (*ETmain*) to keep torque constant while varying also the start of injection (*SOImain*) to keep nearly constant the center of combustion. To do so, when the engine is running, the controller reads via CAN bus the values of Start of Injection (*SOI*) and Energizing Time (*ET*) calculated by the engine control system for all the injections (Pilot, Pre and Main) of each combustion. Then, if the error between target and estimated indicated quantities remains below a calibrated threshold, the RCP system overwrites (via CAN bus) final *SOImain* and *ETmain* with the same values calculated by the standard control (Standard injection pattern). Otherwise, if the error increases, the RCP system overwrites *SOImain* and *ETmain* with new calibrations calculated by two separated PID controllers. Figure 5 reports a scheme of the whole developed controller.
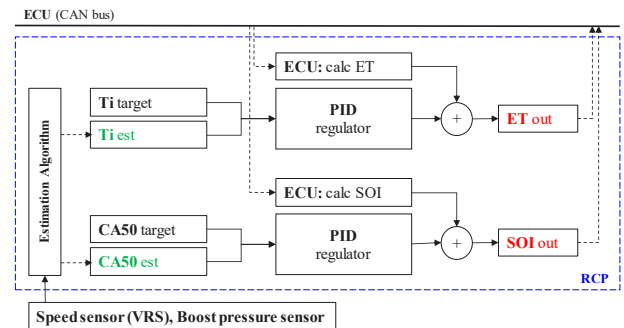

Figure 5: scheme of the closed-loop combustion controller implemented and tested in this study. Here, the estimated indicated quantities are the ones determined from the real-time processing of crankshaft speed fluctuations.

To clarify how the developed controller works, Figure 6 shows the result obtained applying the closed-loop control strategy (that real-time varies the Main injection parameters) during a linear reduction of the amount of diesel injected in the Pilot injection (2-injections pattern).
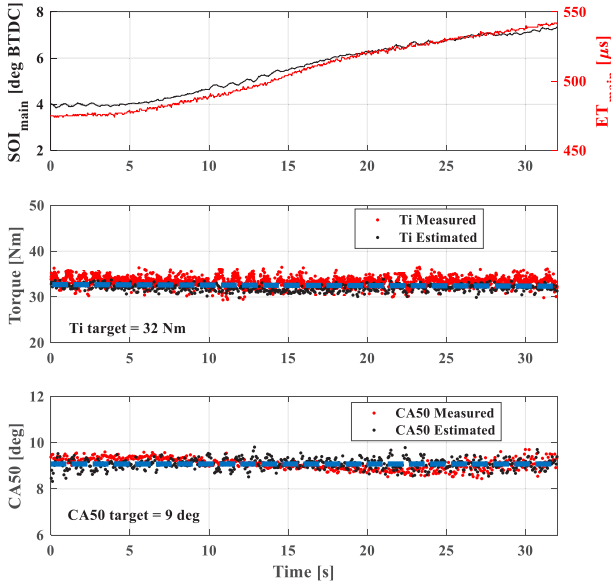
Figure 6: Closed-loop control of SOImain and ETmain while reducing the amount of fuel injected in Pilot from 2.5 to nearly 0 mm3/stroke.

As it can be observed in Figure 6, while the amount fuel injected in the Pilot injection is reduced (from 2.5 to nearly 0 mm3/stroke) the controller increases both *ETmain* and *SOImain* to keep estimated torque and estimated CA50 at their target values. The experimental results demonstrate that the corrections based on the values of the estimated quantities also keep nearly at their target values the actual indicated quantities (calculated by the indicating system from in-cylinder pressure)

Since the center of combustion estimation methodology proved to be effective for the closed-loop control of conventional diesel combustion, further investigations have been performed to extend the approach to other LTC strategy. To do so, the same CI engine has been modified to be operated in PCCI and RCCI mode.

Partially Pre-mixed Compression Ignition (PCCI)

PCCI combustions are diesel CI combustions mainly characterized by high EGR rates and highly premixed combustion portions. The combination of high ignition delays and EGR rates usually results in high sensitivity to cylinder thermal conditions, therefore closed-loop combustion control becomes crucial to guarantee combustion stability [16-19].

To validate the torque and CA50 estimation algorithm for PCCI diesel combustion, the standard injection pattern of the engine under investigation has been significantly modified. The number of injections has been set to 2 (Pilot, Main) and the amount of fuel injected in Pilot injection (*Qpil*) has been increased (up to 4 times the standard value) while reducing *Qmain* (to keep constant the overall fuel consumption). EGR rate has been also increased, the goal being to reduce combustion stability and increase cycle-to-cycle variability. As an example, starting from the standard injection pattern actuated by the ECU while running the engine at 2000 rpm and IMEP = 4 bar, *Qpil* has been increased from 1 to 4 mm3/stroke and *SOIpil* has been

varied from nearly 14 up to 40 deg (while *SOImain* has always been kept constant at 3.5 deg).

The variations applied to the standard injection pattern significantly modify the way energy is released during the combustion process. Figure 7 shows an example of ROHR, calculated through Eq. (5), for an engine cycle in PCCI mode (red) compared to a baseline cycle run in CDC mode using the standard injection pattern (black).

$$ROHR = \frac{1}{\gamma - 1} \cdot V \cdot \frac{dp}{d\theta} + \frac{\gamma}{\gamma - 1} \cdot p \cdot \frac{dV}{d\theta} \qquad (5)$$

For the cycle run in PCCI mode, the oscillations visible in the angular range corresponding to the Main combustion portion is caused by the impulsive energy release (more pre-mixed with respect to CDC), that occurs in a short angular range and produces high frequency oscillations captured by the in-cylinder pressure transducer.
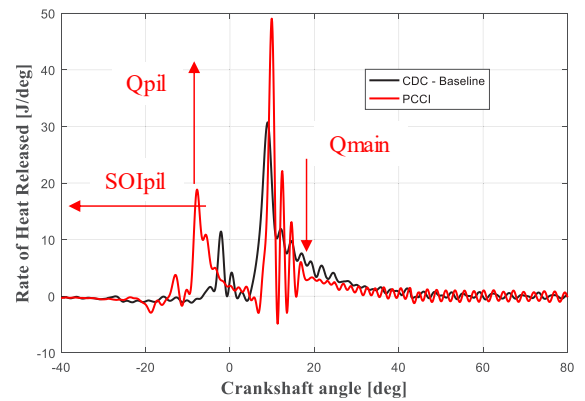

Figure 7: Comparison between ROHR in PCCI and CDC mode. Tests run at 2000 rpm and IMEP = 4 bar.

The whole PCCI combustion process can be often divided in 2 consecutive and partially overlapped combustion events. In this case, the calculated CA50 value becomes very noisy, and might also be unable to provide accurate information about combustion location within the cycle.
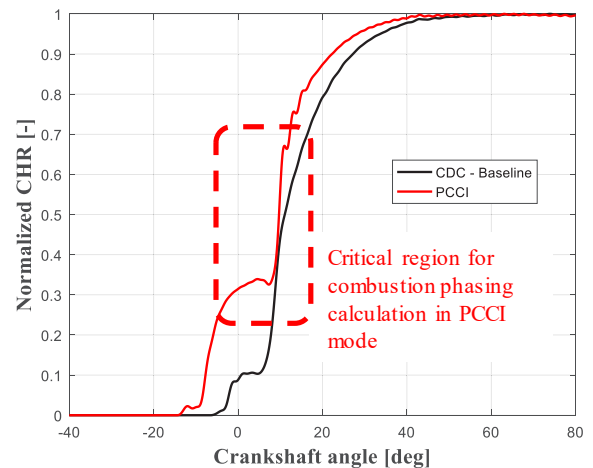

Figure 8: Normalized CHR curve for an engine cycle run at 2000 rpm and IMEP = 4 bar in PCCI mode.

To clarify this consideration, Figure 8 reports the cumulated (net) Rate of Heat Release for an engine cycle run in PCCI mode at 2000 rpm and IMEP = 4 bar. As it can be observed, identifying the angular position corresponding to the 50% of ROHR cumulated sum (CHR) can be critical, mainly due to the high dwell time (that leads to a non-monotonically increasing curve) between Pilot and Main injection. In some cases, this behavior makes CA50 a non-useful parameter for closed-loop combustion control.

Although CA50 calculation might be critical for PCCI combustions, engine speed can still be used to estimate the indicated torque fluctuation of interest. Figure 9 reports the result obtained applying the torque fluctuation estimation methodology. As it can be observed, also in PCCI combustion, both amplitude (still strongly correlated with indicated torque mean value over the engine cycle) and phase of the indicated torque fluctuation can be accurately estimated. This quantity still provides important information about combustion location within the cycle, even if it is not always linearly correlated with CA50.
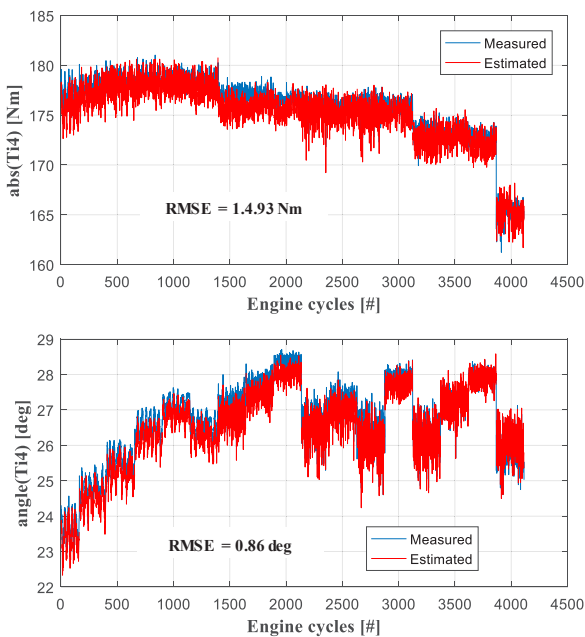

Figure 9. Measured vs Estimated Torque fluctuation (amplitude and phase) for the tests run in PCCI mode at 2000 rpm and IMEP = 4 bar (SOI variations).

Reactivity Controlled Compression Ignition (RCCI)

As mentioned in the previous sections, the remote combustion sensing algorithm based on the analysis of crankshaft speed fluctuation has been also applied to the 1.3L Diesel engine run in RCCI mode.

Even though the analysis of dual-fuel RCCI (gasoline/diesel) combustion is beyond the scope of this work, it is important to highlight that this LTC strategy can be tested only modifying the hardware of the standard injection system. In particular (starting from a CI diesel engine) it is necessary to install and properly manage an additional fuel system for the injection of the low-reactivity fuel (gasoline in this case) [8]. According to Reitz [1,3,20], the intake manifold has been modified installing 4 gasoline PFI injectors, i.e. one per cylinder. The PFI injectors are connected to a rail filled with

gasoline, kept at constant pressure (5.5 bar) and the amount of injected gasoline is pre-mixed with fresh air in the intake manifold. Then, combustion is activated through direct diesel injection, performed using the standard common-rail injectors.

The location of the additional PFI injectors, together with the installation of the additional accelerometer (which signal will be analyzed in the following sections), is shown in Figure 10.
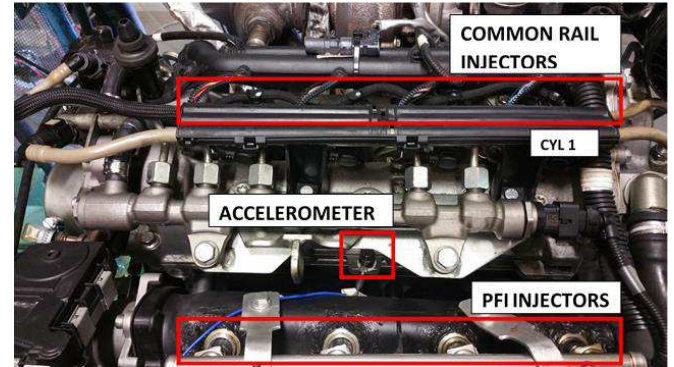

Figure 10. Modified injection system (gasoline and diesel) and accelerometer location.

The control of the additional fuel system for gasoline injection has been implemented in the RCP, that real-time calculates the angular position of the crankshaft using the signal coming from the magnetic pick-up faced to the toothed wheel already present on-board and generates the logical injectors commands, defined as functions of the parameters *ETgas* (gasoline Energizing Time) and *SOIgas* (gasoline Start of Injection). The logical commands (0-12 V) are then converted in electric commands for the PFI injectors using a specific ECU connected to the RCP system. To properly manage RCCI combustion, the experimental layout previously reported in Figure 1 has been modified as shown in Figure 11.
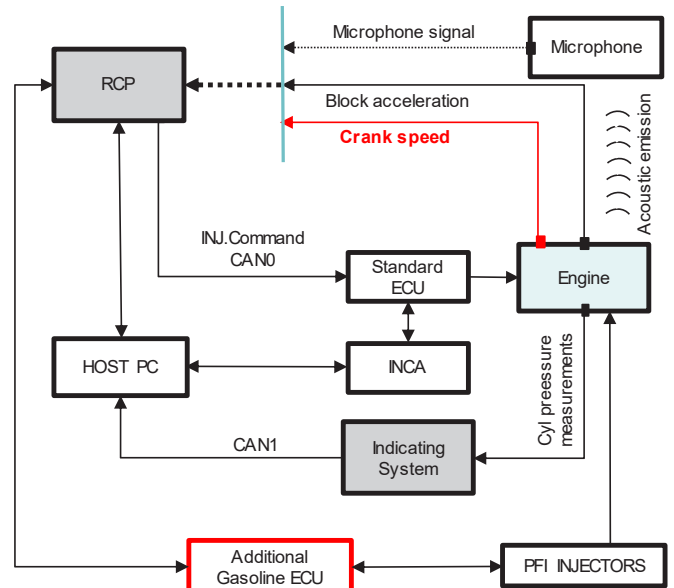

Figure 11. Scheme of the developed experimental setup for the management of RCCI combustion.

1/15/2019

To validate the methodology in RCCI mode, several tests have been run at 2000 rpm and IMEP = 4 bar investigating wide ranges of EGR (from 10% to 32%). In addition, 3 different gasoline/diesel target ratios have been tested: 55/45, 70/30 and 80/20 (the mass of each fuel has been corrected, with respect to the ratio, according to the defferences between the lower heating values of the fuels). During all the tests, the base structure of the diesel injection pattern has been maintained in terms of number of injections and dwell time between injections, while combustion phasing has been modified varying *SOImain* (from 10° TDC up to 45° BTDC). To achieve the mentioned gasoline/diesel target ratios maintaing constant the total amount of energy, the energy introduced with gasoline has been compensated equally reducing *Qmain*.

To better clarify the capability of extracting information about how combustion takes place in RCCI mode, Figure 12 shows the real-time application of the CA50 estimation algorithm to a steady-state test run with gasoline/diesel target ratio 55/45. During the test, *SOImain* has been varied from 5 to 0 deg BTDC (combustion retarded). As already mentioned, in this case the 3-injection pattern is simply shifted, because the Dwell Time between injections is kept constant. As a result, the average apparent heat release over the cycle (ROHR) varies as reported in the top subplot of Figure 12.
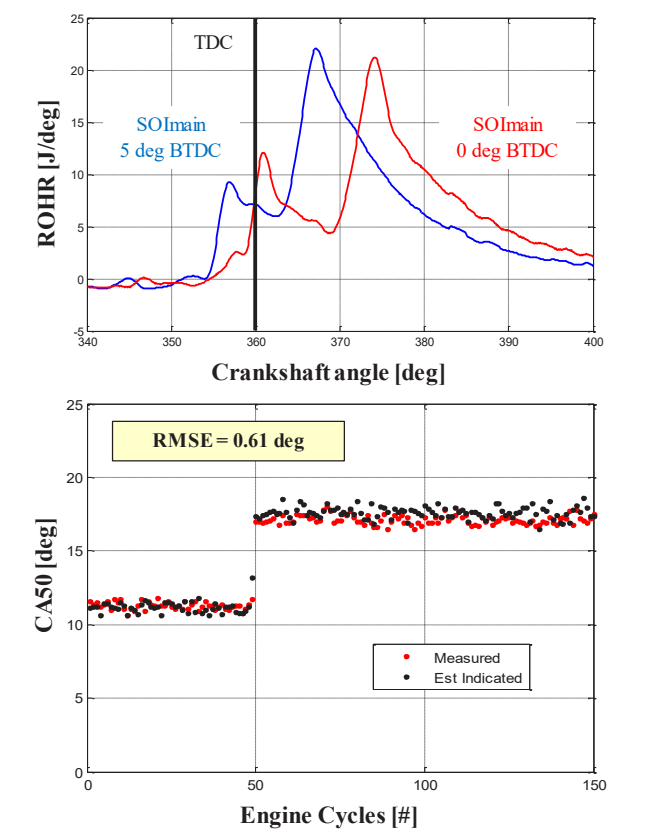

Figure 12. Measured and estimated center of combustion for a test run at 2000 rpm, IMEP = 4 bar, gasoline/diesel target ratio 55/45.

It is important to highlight that in this case the transfer function used is the same previously shown in Figure 3 and determined using a set of transient test run in CDC mode (the transfer function only depends on the torsional characteristics of the system under study).

Then, the estimated values of amplitude and phase of the torque fluctuation have been correlated to average indicated torque and CA50 respectively. Table 2 summarizes the accuracy of the obtained estimations for the 3 gasoline/diesel target ratios analyzed.

Table 2. Accuracy of torque and CA50 estimation for the tests run in RCCI mode.

	Torque RMSE [Nm]	CA50 RMSE [deg]
Gasoline/diesel 55/45	3.42	0.61
Gasoline/diesel 70/30	3.60	0.65
Gasoline/diesel 80/20	4.03	0.72

Analysis of a Spark-Ignited Engine in which Combustions are Not Evenly-Spaced

The engine analyzed in the previous section performs 4 evenly-spaced combustions per cycle, therefore choosing the engine order of interest is easy. In general, selecting the harmonic component characteristic of the engine is straightforward for all the engines that perform a fixed number of evenly-spaced combustions over an engine cycle, because it always corresponds to the number of cylinders [15].

The scenario is completely different for engines with combustions that are not evenly-spaced. In this case, even if torque delivered by all cylinders is the same, torque and speed frequency contents are high in correspondence of different engine orders, depending on number of cylinders, combustion order and angular distance between combustions. To clarify these considerations, a 4-cylinder engine with combustions not evenly-spaced has been analyzed. The engine, coupled to a vehicle (motorcycle application), has been run from 3000 to 12000 rpm at different loads, measuring engine speed and in-cylinder pressure.
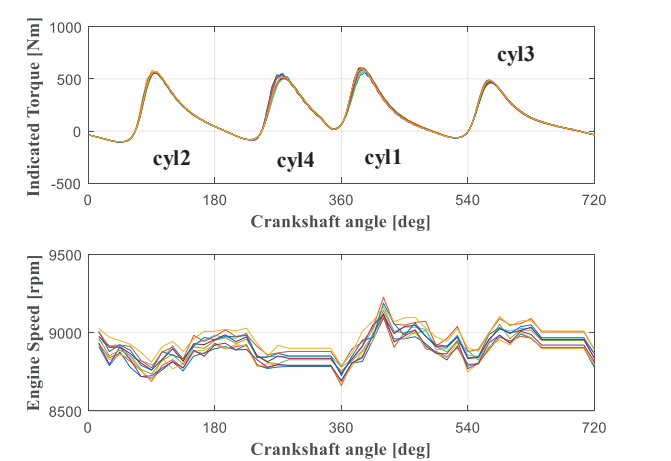

Figure 13. Indicated torque and engine speed during a test run at 9000 rpm in full load.

Figure 13 shows indicated torque and engine speed waveforms during 10 consecutive engine cycles run in full load conditions at nearly 9000 rpm. As it can be observed, combustions are not evenly-

spaced, therefore the amplitude of torque harmonic components remains positive in correspondence of harmonic 1, 3 and 4.

Figure 14 clarifies the above consideration: even if all the cylinders produced the same torque waveform over crank angle, i.e. the only difference between the torque harmonic components were a phase shift related to the firing order (1-3-2-4 in this case), the torque harmonic components ($T_{ind,k}$) for k=1, 3, 4 would still be positive.
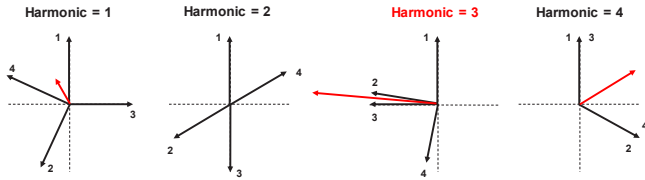

Figure 14. Torque harmonic components up to harmonic 4 for the SI engine in which combustions are not evenly-spaced.

In this case, the selection of the harmonic component of interest cannot be performed a priori. However, Figure 14 clearly suggests that the harmonic component characterized by the highest amplitude, therefore the one with the highest signal to noise ratio, is harmonic 3. For this reason, the transfer function corresponding to the torsional characteristic of the engine-driveline system was calculated in the frequency range corresponding to harmonic 3 [3,15]. Figure 15 shows the obtained results.
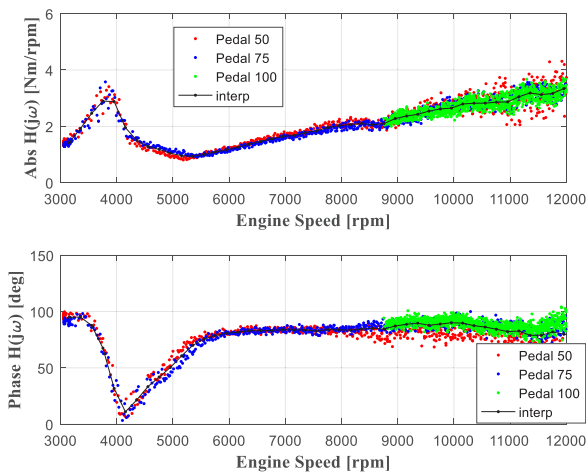

Figure 15. Transfer function characteristic of the SI engine-driveline system.

The calculated transfer function has been implemented in the RCP and finally used to real-time estimate indicated torque and center of combustion. Figure 16 shows that the estimation algorithm proved to be effective also when combustions are not evenly-spaced.
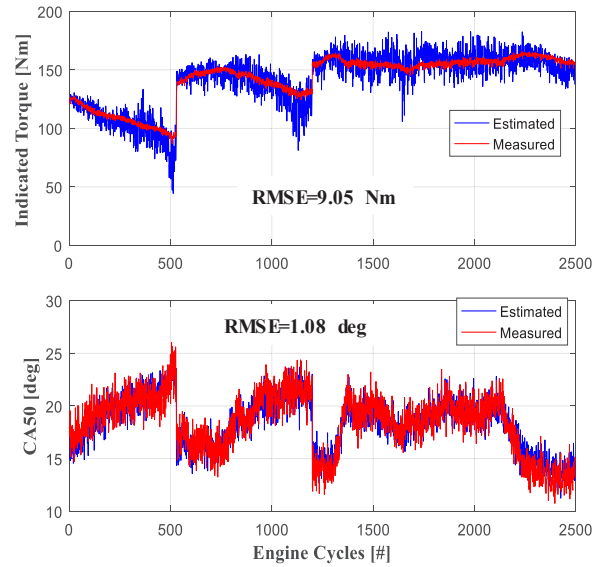

Figure 16. Indicated torque mean value and center of combustion for the SI engine with combustions not evenly-spaced, estimated vs measured..

Pressure Peak Position and SOC Estimation via Accelerometer

Another key source to sense ICE combustion is the engine block vibration sampled by means of an accelerometer. Prior studies [21,22], also performed by the authors [11] demonstrate that accelerometers mounted on the engine block can be used to extract useful information about combustion effectiveness. In this case, the accelerometer signal has been used to determine pressure peak and SOC location within the cycle.

To understand the nature of the correlation between engine block acceleration and the combustion process, Figure 16 shows a comparison between the normalized accelerometer signal and the corresponding normalized cylinder pressure derivative for cylinder 1. Pressure and block acceleration have been acquired running the 4-cylinder CI engine in RCCI mode at 2000 rpm, IMEP = 5 bar and gasoline/diesel target ratio 70/30. Since the goal of the analysis is to extract information about combustion location within the cycle, both in-cylinder pressure and engine block acceleration (coming from the PCB Piezotronic accelerometer installed in the position highlighted in Figure 9) have been low-pass filtered at 3 kHz.

The main idea behind the approach is that cylinder pressure derivative is correlated with combustion velocity, i.e. to the way energy is released during the combustion process. Since the accelerometer perceives the block acceleration due to the impulsiveness of combustion, it is reasonable to expect that a correlation with cylinder pressure derivative can be set up. According to Figure 17, the maximum value of block acceleration corresponds to the angular position in which cylinder pressure shows the maximum pressure rise rate (that can be considered a good approximation of combustion start), while the following zero-crossing is a good estimator of the pressure peak location.
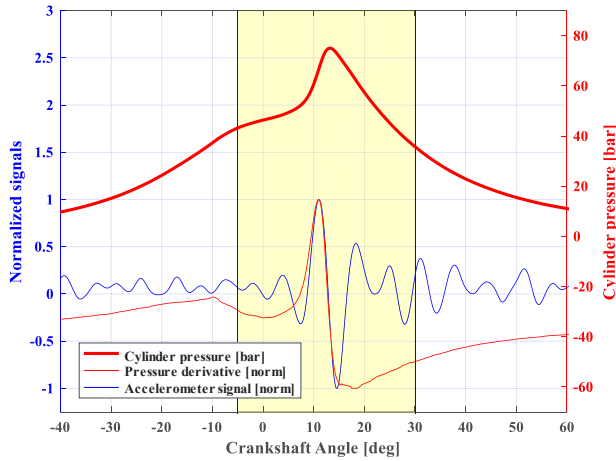
Figure 17. In-cylinder pressure, in-cylinder pressure first derivative and engine block acceleration (normalized with respect to their maximum) for a test run in RCCI mode at 2000 rpm, IMEP approximately 5 bar and gasoline/diesel target ratio 70/30.

To obtain the proper correspondence between acceleration and pressure derivative it is necessary to compensate the time delay of the acceleration signal, i.e. the delay between the moment at which combustion occurs and the one at which the accelerometer perceives the effects. Such time delay is nearly constant over the entire engine operating range and mainly depends on the distance between the accelerometer and each cylinder (obviously the constant time delay becomes variable in the angular domain while engine speed varies). Once the accelerometer delay (with respect to the combustion process of each cylinder) has been identified, it is possible to compensate the delay and properly window the signal to extract the information about pressure peak location and SOC [11].

As already mentioned, to estimate pressure peak location and SOC it is necessary to compensate the delay and properly window the block acceleration signal to minimize detection errors (mainly due to mechanical vibrations, always captured by the accelerometer). Then, pressure peak location and SOC can be easily detected through an algorithm that identifies the angular positions (within the cycle) corresponding to the maximum of the windowed acceleration signal and the following zero-crossing. Such algorithm has been implemented in the RCP system and applied to the combustion methodologies discussed in the previous sections. With regard to the selection of the observation window, in this work a Tukey window with variable angular duration has been implemented [11]. The angular duration has been defined as a function of engine speed and load.

The discussed algorithm proved to be effective for pressure peak location (strongly correlated with CA50 [27]) and SOC estimation in all the engines under investigation. As an example, Figure 18 shows the results obtained during a transient test performed running the CI engine in CDC mode. The accuracy of the obtained results is high enough to feedback an algorithm for closed-loop combustion control.
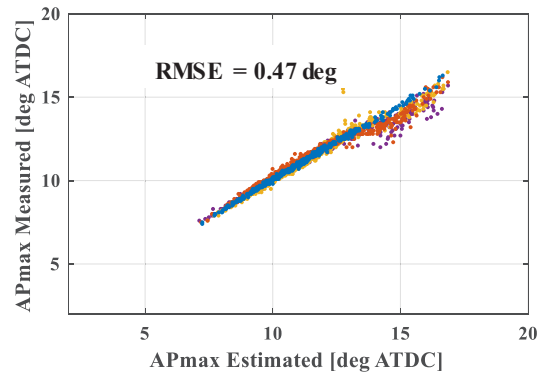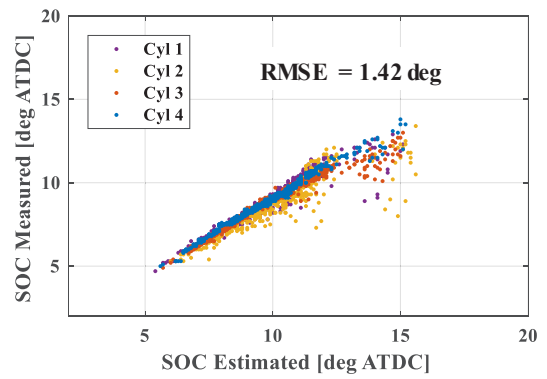
Figure 18. Estimation of pressure peak and SOC during transient test run in CDC mode.

The same methodology has been validated also running the engine in RCCI mode, obtaining similar results. Figure 19 summarizes the results of the real-time pressure peak estimation for tests run at 2000 rpm and IMEP = 4 bar in RCCI mode performing a sweep of EGR ratio.
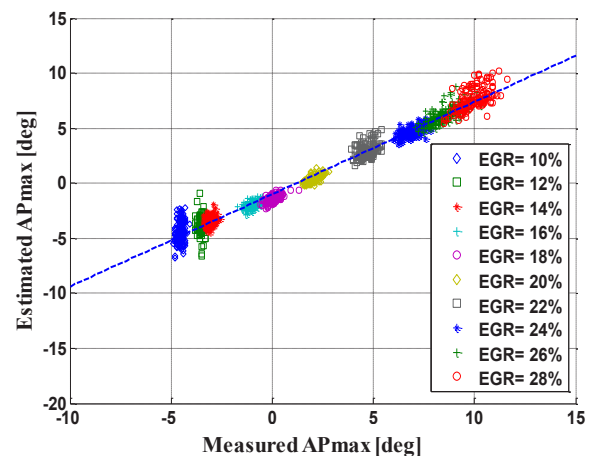

Figure 19. Estimation of pressure peak location for tests run in RCCI mode performing an EGR scan.

Due to the highly pre-mixed portions, the approach needs to be slightly modified to properly manage PCCI combustions. As already discussed, the PCCI combustion process can be usually divided in 2 consecutive (partially overlapped) combustion events. As a result, the major peak in the accelerometer signal might be caused by both premixed and diffusive combustion portion. To manage this peculiar behavior, the algorithm has been modified to capture the maximum and the following zero-crossing of the 2 major peaks in the acceleration signal. To clarify this consideration Figure 20 shows the detection of the 2 peaks of interest for a test run at 2000 rpm and IMEP = 4 bar in PCCI mode.
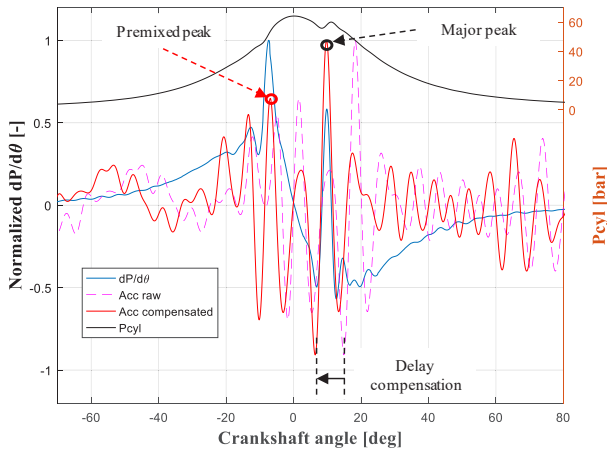

Figure 20. Application of the algorithm for the detection of accelerometer peaks location, engine cycle run in PCCI mode.

It is important to highlight that the detection of combustion phasing based on accelerometer processing is not influenced by engine layout or combustion order, since the combustion process of each cylinder is windowed. In this case, the main limitation is the signal-to-noise ratio, that might be too low to guarantee a robust estimation when the amplitude of mechanical vibrations is equal or higher than the amplitude of the vibrations caused by the combustion process. The signal-to-noise ratio can be usually improved increasing the number of accelerometers applied to the engine block. However, the accuracy of the algorithm is usually low during high speed (high amplitude of mechanical vibrations) or low load (low amplitude of combustion vibrations) operating conditions.

Combustion Noise control via Acoustic Emission Real-Time processing

The last part of this paper describes a methodology for the calculation of engine noise, that provides a potential for the control of Common Rail Multi-Jet diesel engines.

As it is well known, engine noise is usually monitored calculating the Combustion Noise (CN) index, that can be directly calculated from in-cylinder pressure trace. Many works [23-25] demonstrate that combustion noise is strongly influenced by the impulsiveness of the combustion process, because fast pre-mixed diesel combustions (with high ROHR peaks) are usually characterized by high CN values. To verify this, a set of experimental tests has been performed running the CI engine under study in CDC conditions. All the operating points (summarized in Table 3) have been run both using the standard

injection pattern (3 injections) and switching off both Pilot and Pre injections (only one Main injection, with increased amount of fuel injected to compensate Pilot and Pre omission).

Table 3. Tests run in CDC mode for the analysis of the acoustic emission.

Rpm	IMEP [bar]			
	3	6	9	12
1250	1	2	3	4
1500	5	6	7	8
2000	9	10	11	12
2500	13	14	15	16

The set of experimental data confirms that CN, calculated using the algorithm proposed in [26], is strongly correlated to combustion impulsiveness, because it is well correlated with the maximum amplitude of cylinder pressure first derivative or with the maximum ROHR peak. As reported in Figure 21, for each operating point, the impulsive combustion (higher cylinder pressure derivative) is always characterized by a higher combustion noise.
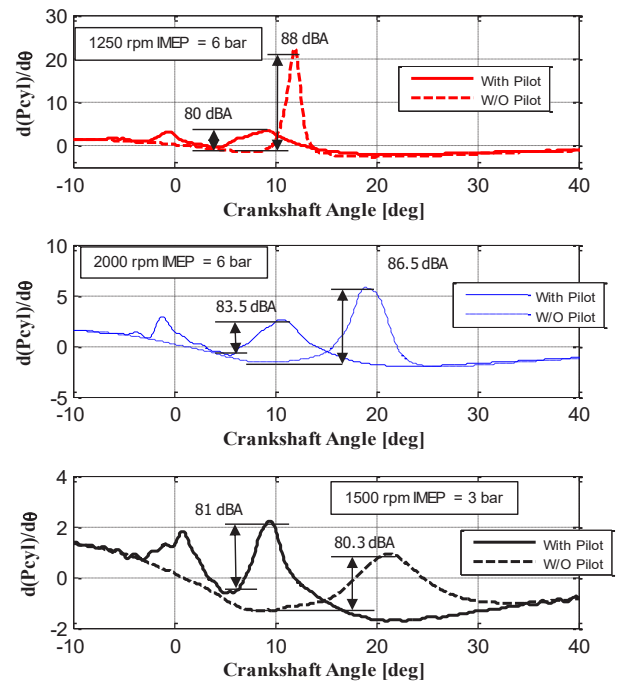
Figure 21. Comparison between cylinder pressure derivatives and corresponding Combustion Noise for engine cycles run in CDC mode with standard injection pattern (3 injections) and without pre-injections.

Although CN shows a good correlation with pressure derivative and ROHR peak, the goal of the approach presented in this work is to provide an algorithm for the closed-loop control of engine noise based on the real-time processing of the signal coming from the microphone faced to the engine block. To do so, it is necessary to consider that the microphone perceives the overall noise radiated by the engine, i.e. the sum of combustion noise (CN) and mechanical

noise (MN). To quantify the overall noise radiated by the engine, Eq. (6) has been implemented in the RCP.

$$Noise = CN + MN = log_{10}\left(\frac{\bar{E}}{\bar{E}_0}\right) \qquad (6)$$

Here, $\bar{E}$ is the mean energy level of the signal (evaluated from the spectrum of the acoustic emission signal), while $\bar{E}_0$ is a standard reference value that corresponds to the energy level at 20 µPa, which is usually considered the threshold of human hearing at 1 kHz [25].

Since mechanical noise is produced by the mechanical components in motion, it is mainly influenced by the engine rotational speed. As a result, the overall noise is a function of both engine speed and combustion impulsiveness (ROHR peak). Figure 22 shows that the correlation between overall noise and ROHR peak is nearly linear. However, given a value of ROHR peak, the overall noise level rises with engine speed. To highlight the effect of engine speed (mechanical noise) on the overall radiated noise, the linear fittings reported in Figure 22 are all characterized by the same slope, while a noise offset (mechanical noise variation) is applied to properly fit the experimental measurements.
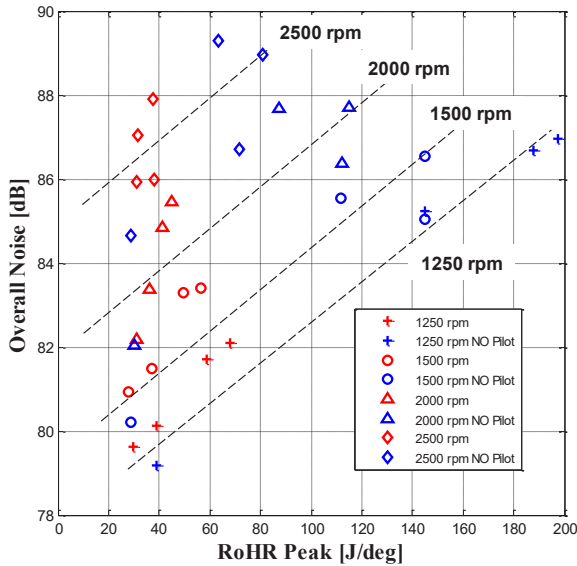

Figure 22. Correlation between overall noise radiated by the CI engine run in CDC mode (measured using the acoustic sensor) and ROHR peak. Test run with standard injection pattern and omitting pre-injections.

According to the discussed results, the use of a microphone allows the indirect calculation of CN. Once mechanical noise has been identified (mainly as a function of engine speed) the overall noise target needs to be set taking into consideration mechanical noise variations with engine speed.

Previous works by the same authors demonstrate that [12] it is possible to real-time control engine noise (overall) properly activating or omitting pre-injections (Pilot or Pre). The dynamic variation of the injection pattern (limited by the measured noise) provides a significant potential in the reduction of pollutant emissions, especially particulate matter [26], because while combustions performed without pre-injections are usually

characterized by an unacceptable engine noise, soot emissions usually drop with respect to the corresponding operating conditions run with Pilot and Pre. The main idea behind the proposed approach is that the noise (and consequently pollutant emissions) can be controlled running the engine in an intermediate operating mode in which Pilot and Pre are removed only to a subset of the total number of combustions performed, according to a proper designed sequence of engine cycle over a generic N-cycles buffer [12]. The switching frequency between the two operating modes (standard with Pilot and Pre or modified activating only the Main injection) needs to be high enough to produce noise discontinuities that can be barely perceived by the driver. Once N is fixed, N+1 options become available to properly design the sequence. Each sequence corresponds to an intermediate level between standard (3 injections) and modified (only one injection) injection patterns. To clarify this consideration, Eq. (7) reports a matrix that contains 8 injection sequences that can be designed for N = 7.

$$Sequences_{N=7} = \begin{bmatrix} 0000000 \\ 0001000 \\ 0010010 \\ 0101010 \\ 1010101 \\ 1101101 \\ 1110111 \\ 1111111 \end{bmatrix} \qquad (7)$$

A noise control algorithm has been implemented in the RCP system and tested in dynamic conditions. This methodology real-time varies the sequence of standard and modified combustions based on the error between target and measured noise (calculated through Eq. (6) from the microphone signal). As it can be observed in Figure 23, the selection of the proper injection pattern (performed by a PID controller) always allows controlling the target noise level, except in the cases in which the noise target is higher or lower with respect to the reachable noise levels.

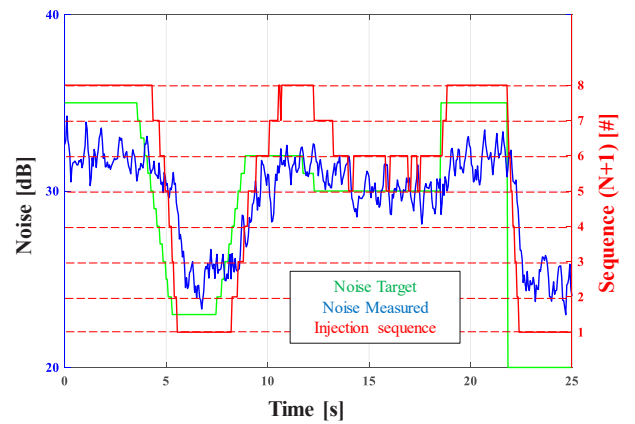Figure 23. Noise produced by the engine (while activating the noise control algorithm) together with the selected injection sequence.

Summary/Conclusions

This paper reviews several algorithms for remote combustion sensing developed by the authors over the past years. The discussed methodologies extract indicated quantities, usually directly calculated from in-cylinder pressure measurement, using low-cost sensors

applied to the engine. In particular, to estimate torque, combustion phasing (center of combustion, pressure peak location and SOC) and combustion noise, the discussed procedures use the standard phonic wheel already present on-board for other control purposes, one additional accelerometer and one microphone.

The complete remote combustion sensing methodology has been implemented in a programmable rapid control prototyping (RCP) system and applied to different combustion methodologies (both conventional and LTC) and engine architectures.

The proposed algorithms proved to be effective in all the analyzed cases, and the accuracy of the estimated combustion indexes seems to be accurate enough to feedback an algorithm for closed-loop combustion control, i.e. an algorithm that real-time varies the ignition/injection parameters to keep the estimated combustion feedbacks at the proper target value. For generic engine applications, the accuracy of the discussed algorithms cannot be defined a priori, because it will be strongly dependent on the signal-to-noise ratio characteristic of the specific application, i.e. on the capability of perceiving the effects of combustion using the analyzed low-cost sensors. However, this work clearly highlights the potential of the discussed approaches when implemented in a real-time system (RCP).

Additional work has been done to implement the developed algorithms in standard ECUs for on-board engine control, to prove that there is no limitation related to the on-board installation. Further studies are also being performed on an engine-dyno system to define the operating ranges in which a reliable combustion optimization can be guaranteed over time.

References

1. Curran, S., Hanson, R., Wagner, R., and Reitz, R., "Efficiency and Emissions Mapping of RCCI in a Light-Duty Diesel Engine," SAE Technical Paper 2013-01-0289, 2013, doi:10.4271/2013-01-0289.
2. Kimura, S., Aoki, O., Kitahara, Y., Aiyoshizawa, E., "Ultra-Clean Combustion Technology Combining a Low-Temperature and Premixed Combustion Concept for Meeting Future Emission Standards", SAE Paper 2001-01-0200.
3. Kokjohn, S., Hanson, R., Splitter, D., and Reitz, R., "Experiments and Modeling of Dual-Fuel HCCI and PCCI Combustion Using In-Cylinder Fuel Blending," *SAE Int. J. Engines* 2(2):24-39, 2010, doi:10.4271/2009-01-2647.
4. Schnorbus, T., Pischinger, S., Körfer, T., Lamping, M. et al., "Diesel Combustion Control with Closed-Loop Control of the Injection Strategy," SAE Technical Paper 2008-01-0651, 2008, doi:10.4271/2008-01-0651.
5. Kolbeck, A.F., "Closed Loop Combustion Control - Enabler of Future Refined Engine Performance Regarding Power, Efficiency, Emissions & NVH under Stringent Governmental Regulations", SAE Technical Paper 2011-24-0171, 2011, doi:10.4271/2011-24-0171.
6. Wu Y, Hanson R, Reitz RD., "Investigation of Combustion Phasing Control Strategy During Reactivity Controlled Compression Ignition (RCCI) Multicylinder Engine Load Transitions". *ASME. J. Eng. Gas Turbines Power*. 2014;136(9):091511-091511-10. doi:10.1115/1.4027190.
7. Kokjohn, S. L., Hanson, R. M., Splitter, D. A., Reitz R. D., "Fuel reactivity-controlled compression ignition (RCCI): a pathway to controlled high-efficiency clean combustion",
International Journal of Engine Research, Vol 12, Issue 3, pp. 209 – 226, First published date: June-22-2011.
8. Ravaglioli, V., Ponti, F., De Cesare, M., Stola, F. et al., "Combustion Indexes for Innovative Combustion Control," *SAE Int. J. Engines* 10(5):2371-2381, 2017, doi:10.4271/2017-24-0079.
9. Ponti, F., Ravaglioli, V., Serra, G., and Stola, F., "Instantaneous Engine Speed Measurement and Processing for MFB50 Evaluation," *SAE Int. J. Engines* 2(2):235-244, 2010, doi:10.4271/2009-01-2747.
10. Ponti, F., Ravaglioli, V., Moro, D., Serra, G., "MFB50 on-board estimation methodology for combustion control," *Control Engineering Practice*, 2013, 21, pp. 1821 – 1829, doi:10.1016/j.conengprac.2013.05.001.
11. Ponti, F., Ravaglioli, V., Cavina, N., De Cesare, M., "Diesel Engine Combustion Sensing Methodology Based on Vibration Analysis". ASME. *J. Eng. Gas Turbines Power*. 2014;136(11):111503-111503-7. doi:10.1115/1.4027363.
12. Ponti, F., Ravaglioli, V., Stola, F., and De Cesare, M., "Engine Acoustic Emission Used as a Control Input: Applications to Diesel Engines," SAE Technical Paper 2016-01-0613, 2016, doi:10.4271/2016-01-0613.
13. Ponti, F., De Cesare, M., and Ravaglioli, V., "Development and Validation of a Methodology for Real-Time Evaluation of Cylinder by Cylinder Torque Production Non-Uniformities," SAE Technical Paper 2011-24-0145, 2011, doi:10.4271/2011-24-0145.
14. Ponti, F., Ravaglioli, V., De Cesare, M., Stola, F., "Torque and Center of Combustion Evaluation Through a Torsional Model of the Powertrain". ASME. *J. Dyn. Sys., Meas., Control*. 2015;137(6):061005-061005-9. doi:10.1115/1.4029195.
15. Ravaglioli, V., Ponti, F., and Stola, F., "Torsional Analysis of Different Powertrain Configurations for Torque and Combustion Phase Evaluation," SAE Technical Paper 2011-01-1544, 2011, doi:10.4271/2011-01-1544.
16. Reitz R.D., Duraisamy G., "Review of high efficiency and clean reactivity controlled compression ignition (RCCI) combustion in internal combustion engines," *Progress in Energy and Combustion Science* (2014), doi:10.1016/j.pec20s. 14.05.003.
17. Kanda, T., Hakozaki, T., Uchimoto, T., Hatano, J. et al., "PCCI Operation with Early Injection of Conventional Diesel Fuel," SAE Technical Paper 2005-01-0378, 2005, doi:10.4271/2005-01-0378.
18. Hardy, W. and Reitz, R., "A Study of the Effects of High EGR, High Equivalence Ratio, and Mixing Time on Emissions Levels in a Heavy-Duty Diesel Engine for PCCI Combustion," SAE Technical Paper 2006-01-0026, 2006, doi:10.4271/2006-01-0026.
19. Torregrosa, A.J.; Broatch Jacobi, J.A.; García Martínez, A.; Monico Muñoz, L.F. (2013). "Sensitivity of combustion noise and NOx and soot emissions to pilot injection in PCCI Diesel engines," *Applied Energy*. 104:149-157. doi:10.1016/j.apenergy.2012.11.040.
20. Gross, C. and Reitz, R., "Investigation of Steady-State RCCI Operation in a Light-Duty Multi-Cylinder Engine Using "Dieseline"," SAE Technical Paper 2017-01-0761, 2017, doi:10.4271/2017-01-0761.
21. Polonowski, C., Mathur, V., Naber, J., and Blough, J., "Accelerometer Based Sensing of Combustion in a High Speed HPCR Diesel Engine," SAE Technical Paper 2007-01-0972, 2007, doi:10.4271/2007-01-0972.
22. Arnone, L., Boni, M., Manelli, S., Chiavola, O. et al., "Block Vibration Measurements for Combustion Diagnosis in Multi-Cylinder Common Rail Diesel Engine," SAE Technical Paper 2009-01-0646, 2009, doi:10.4271/2009-01-0646.

1/15/2019

23. Busch, S., Zha, K., Miles, P., Warey, A. et al., "Experimental and Numerical Investigations of Close-Coupled Pilot Injections to Reduce Combustion Noise in a Small-Bore Diesel Engine," *SAE Int. J. Engines* 8(2):660-678, 2015, doi:10.4271/2015-01-0796.

24. Busch, S., Zha, K., Miles, P., Warey, A. et al., "Experimental and Numerical Investigations of Close-Coupled Pilot Injections to Reduce Combustion Noise in a Small-Bore Diesel Engine," *SAE Int. J. Engines* 8(2):2015, doi:10.4271/2015-01-0796.

25. Ponti, F., Ravaglioli, V., Moro, D., and De Cesare, M., "Diesel Engine Acoustic Emission Analysis for Combustion Control," SAE Technical Paper 2012-01-1338, 2012, doi:10.4271/2012-01-1338.

26. Shahlari, A., Hocking, C., Kurtz, E., and Ghandhi, J., "Comparison of Compression Ignition Engine Noise Metrics in Low-Temperature Combustion Regimes," *SAE Int. J. Engines* 6(1):541-552, 2013, doi:10.4271/2013-01-1659.

27. Ravaglioli, V., Stola, F., De Cesare, M., Ponti, F. et al., "Injection Pattern Design for Real Time Control of Diesel Engine Acoustic Emission," *SAE Int. J. Commer. Veh.* 10(1):308-316, 2017, doi:10.4271/2017-01-0596.

Definitions/Abbreviations

CA50	Center of combustion
SOC	Start of combustion
ROHR	Rate of heat released
CN	Combustion noise
CDC	Conventional diesel combustion
CI	Compression-ignited
SI	Spark-ignited
PCCI	Premixed-charge compression ignition
RCCI	Reactivity-controlled compression ignition
RCP	Rapid control prototyping
IMEP	Indicated mean effective pressure
SOI	Start of injection
ET	Energizing time
EGR	Exhaust gas recirculation
BTDC	Before top dead center
$T_{ind,k}$	k-th harmonic component of indicated torque
$T_{ind\,cutoff,k}$	k-th harmonic component of indicated torque during a reference cutoff cycle
$T_{r,k}$	k-th harmonic component of reciprocating torque
θ	Crankshaft angle
V	In-cylinder volume
p	In-cylinder pressure
γ	Specific heat ratio
$\dot{\theta}_k$	k-th harmonic component of engine speed
$\dot{\theta}_0$	Average engine speed
p_{man}	Manifold pressure
k_1	Correlation coefficient between manifold pressure and amplitude of the torque harmonic component of interest
k_2	Correlation coefficient between engine speed and amplitude of the torque harmonic component of interest
$\dot{\theta}_{cutoff,k}$	k-th harmonic component of engine speed torque during a reference cutoff cycle
$H(j\omega)$	Transfer function characteristic of the engine-driveline system under study
$\overline{E}_0$	Standard reference value that corresponds to the energy level at 20 μPa
LTC	Low temperature combustions